

**Assessment of structural and hemodynamic performance  
of vascular stents modelled as periodic lattices**

**Purnendu K. M. Prithipaul<sup>1</sup>, Michael Kokkolaras<sup>2</sup>, Damiano Pasini<sup>3\*</sup>**

Department of Mechanical Engineering

McGill University

<sup>1</sup>purnendu.prithipaul@mail.mcgill.ca

<sup>2</sup>michael.kokkolaras@mcgill.ca

<sup>3</sup>damiano.pasini@mcgill.ca

\*corresponding author

## **1 Abstract**

This work considers vascular stents with tubular geometry assumed to follow a periodic arrangement of repeating unit cells. Structural and hemodynamic metrics are presented to assess alternative stent geometries, each defined by the topology of the unit cell. Structural metrics include foreshortening, elastic recoil and radial stiffness, whereas hemodynamic performance is described by a wall shear stress index quantifying the impact of in-stent restenosis. A representative volume element (RVE) modelling approach is used, and results are compared to those obtained from full simulations of entire stents. We demonstrate that the RVE approach can be used to quantify the impact of the topology of the repeating unit on the structural and hemodynamic properties of a stent, and thus support clinicians in making proper choices among alternative stent geometries.

Keywords: stent; lattice; structural performance; hemodynamic performance

## **2 Introduction**

Coronary heart disease is the most common type of heart disease and the leading cause of death in the developed world [1]. It is mainly caused by the development of an atherosclerotic lesion in an artery. The lesion results in plaque build-up along the inner walls of the artery and eventually leads to an occlusion, restricting blood flow. A common treatment is angioplasty, which involves inserting percutaneously a balloon at the end of a catheter into the site of the occlusion. The balloon is then inflated to increase the size of the lumen to restore blood flow. As a result, restenosis can follow immediately after the procedure due to the elastic recoil of the vessel. This may be prevented by using a stent (a tubular scaffold) to support the blood vessel from the inside of the lumen. Stents were introduced in the early 90's, and have been successful at reducing angioplasty-related restenosis [2]. They can also be used to provide support for arterial grafting or aortic valve replacement. Despite a large variety of stent designs in the market, adverse biological responses, such as in-stent restenosis, have not been addressed adequately. While the causes of restenosis are not completely understood, several studies have shown that low shear stress at the arterial wall is one of the main causes [3-6].

Three main mechanical properties govern the structural function of a stent: radial stiffness, elastic recoil and foreshortening [7]. Higher radial stiffness is desired to prevent collapse of the stent, once it is in place. Foreshortening refers to the change in length of the stent upon expansion. During deployment, a desirable property is that the stent has zero foreshortening and low elastic recoil. Placement accuracy is not a trivial matter for the clinical practitioner [8]. A change in length may result in missing the lesion, thus increasing complications requiring further procedures.

Various mechanical stent properties have been studied, including foreshortening, recoil, radial stiffness and fatigue. These attributes have been investigated by means of finite element analysis and experimental investigation [9-18]. Stents with geometry represented by a periodic arrangement of

structural units are often studied [14, 19, 20]. The study of a single unit cell has the advantage of reducing the computational effort that would be required to analyse the entire geometry of the stent. In this manner, the mechanical properties of a stent can be quantified with reduced analysis of its unit cell. For instance, Tan et al. quantified the impact of stent cell geometry on compliance and foreshortening, compromising of voids and struts, such as in a lattice [14]. Finite element analysis was used to systematically compare dissimilar cell geometries and attain desired deformation characteristics. Recently, Douglas et al. followed this approach to study the expansion mechanism of balloon expandable vascular stents without considering their hemodynamic performance [19]. Based on the assumption that the stent consists of repeating units, analytic and kinetic models were developed to quantify foreshortening. Finite element analysis was used to compute radial compliance and recoil for a variety of stents.

Blood flow has a substantial impact on stent restenosis. In most cases, restenosis after a coronary stent implantation is due to the thickening of the intima of the blood vessel, i.e., intimal hyperplasia [2]. Intimal hyperplasia is often observed at specific locations in the stented region [21]. It has been observed that regions of moderate to high shear stress are spared of intimal thickening, while focal lesions develop only in areas of low and recirculating flow [22]. This is the result of a dramatic alteration to the arterial geometry following the implantation of a stent. The change directly affects the velocity profile of the blood flowing through, thereby resulting in a change in the distribution of wall shear stress (WSS) along the entire length of the stented artery [23].

To assess the hemodynamic performance of a stent following implantation, Mejia et al. [24] introduced a set of metrics based on the statistical moments of the WSS distribution, which have been shown to be promising in correctly assessing the performance of the strut profiles of several stents. In addition, they showed that *“appropriate strut apposition can lead to a significant improvement in terms of the hemodynamic performance of a stent”*. This suggests that modifying the design of the stent can improve its hemodynamic performance. A number of studies have investigated the effect of stent design on the distribution of WSS [23, 25-29]. Previous work [24] is limited to stent profiles of a single strut and cannot quantify the critical role of a given struts' layout within the unit cell.

This work focuses on the role the unit cell topology plays on the mechanics and hemodynamic performance of stents. Our objective is to assess their structural and hemodynamic performance via a unit cell approach (or representative volume element - RVE). The existing literature does not include any methodology to quantify the hemodynamic compatibility of stents using a single metric. The main objective of this paper is to introduce a metric for assessing the hemodynamic performance of a stent during the design process.

The next section outlines the approach used to model five common stent designs via an RVE formulation. The computational approach used to model blood flow through a stented vessel is presented in Section 3.3. Statistical moments are used to characterise the distribution of wall shear stress and define a metric to assess hemodynamic performance. The results of the modelling approach are reported and discussed in Section 4 before the conclusions in Section 5.

### **3 Stent modelling using representative volume elements**

The stent designs considered in this work are periodic arrangements of closed unit cells, similar to a tessellation of cells along independent directions that is typical of lattice materials. As with any lattice, the properties of a stent of this kind can be specifically tailored by controlling the topology of its repeating unit.

Performing full-scale finite element analysis of a periodic domain is generally computationally expensive, especially if it is used repeatedly in design optimization studies. It is more appropriate to

resort to homogenization schemes that model a single unit cell as representative of the overall domain response. This is feasible if the unit cell size is sufficiently small relative to the size of the periodic structure. Applying such a method involves imposing assumptions that are equivalent to considering that the size of the RVE is negligible with respect to the size of the macroscopic domain of the lattice [20, 30-38].

Figure 1 illustrates the methodological approach followed in this work, where the structural finite element model and the computational fluid dynamics model are built using only the RVE. An additional advantage of this strategy is that parametric models of a stent can be easily created from the parameterization of a single unit.

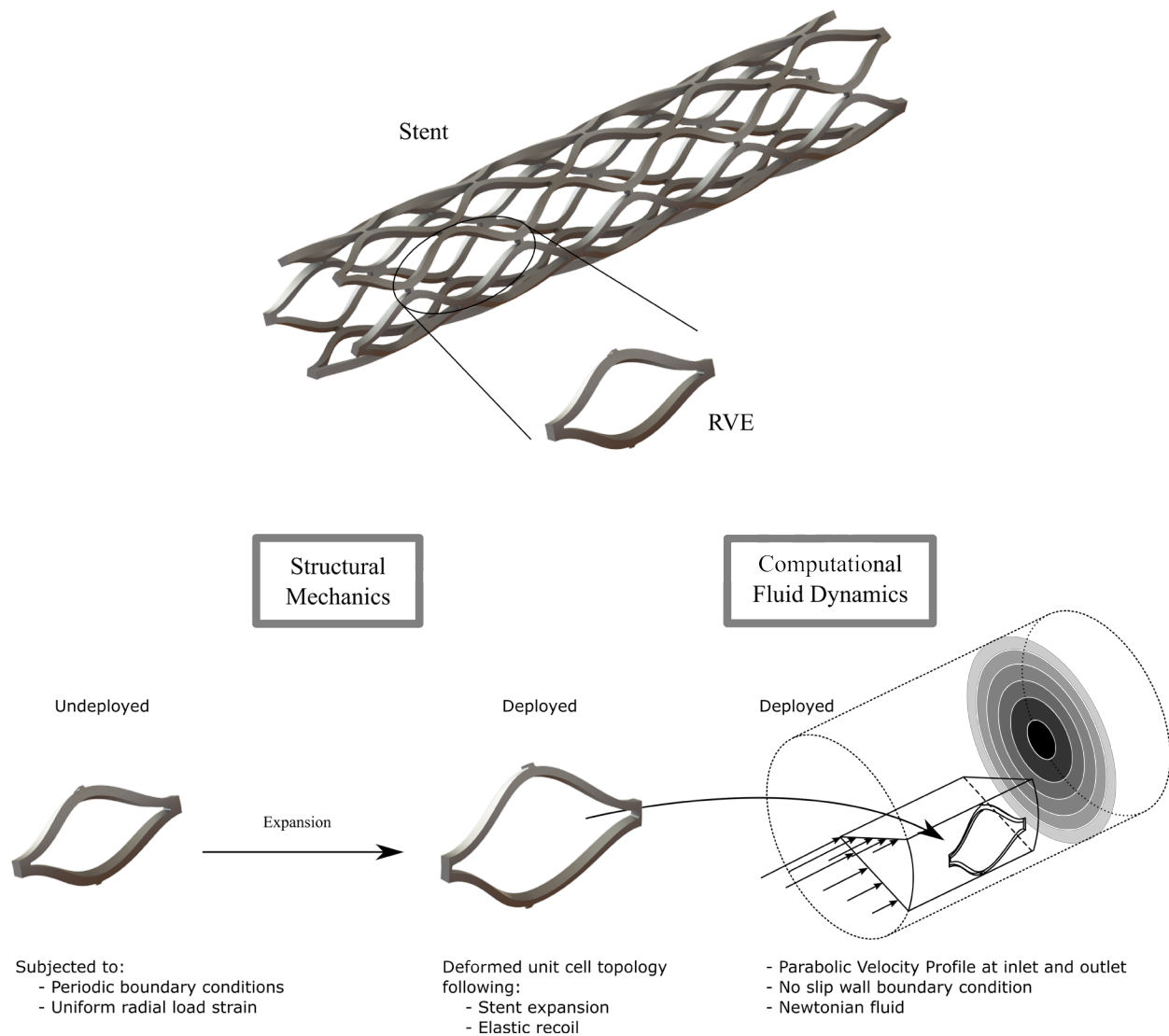


Figure 1: Schematic of the Stent Modelling Approach

### 3.1 Choice of stent unit topology

As in the recent work of Douglas et al. [19], we examine five stent designs, whose unit cells are depicted in Table 1. Other stent parameters are listed in Table 2. We assume that the stents are made of an elastoplastic material with elastic modulus  $E = 193$  GPa, yield strength  $\sigma_y = 260$  MPa, tangential modulus  $E_t = 0$  GPa and Poisson ratio  $\nu = 0.3$  [39]. To simplify the numerical models, the interaction between the wall and atherosclerotic plaque is ignored.

Table 1: Unit cell size and number of cells in radial and circumferential directions


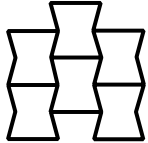
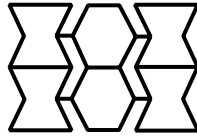
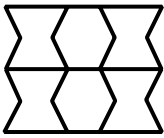
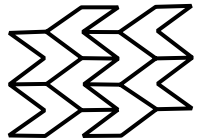
Unit cell	RVE Size		No. of cells	
	$H(\text{mm})$	$L(\text{mm})$	Axial, $N_A$	Circumference, $N_C$
 Diamond	1.047	10	5	12
 Auxetic	2.094	10	5	6
 Hybrid A	2.094	25	2	6
 Hybrid C	1.571	10	3	8
 Chevron B	2.094	10	3	6

Table 2: Stent Parameters

Parameter	Value (mm)
Stent Initial length, $L$	50
Nominal Strut length, $L_{st}$	5
Strut Thickness, $t$	0.4
Initial Diameter, $D_i$	4

Final Diameter, $D_f$	18
-----------------------	----

### 3.2 Stent model and boundary conditions for structural analysis

A stent is implanted using a balloon catheter. The balloon is expanded to plastically deform the stent in place. For this work, the load on the stent is assumed to be entirely radial. The forces exerted in the axial direction by the balloon, artery wall and blood flow are neglected. The expansion mechanism can therefore be modelled by applying a radial strain to the stent. When using an RVE approach, periodic boundary conditions are generally applied to ensure compatibility of deformation and correct computation of stress and strain. The repeating unit is subjected to 3D periodic boundary conditions, expressed using a cylindrical coordinate system by:

$$u_\theta(r, 0, z) = -u_\theta\left(r, \frac{\pi}{N_c}, z\right) \quad (1)$$

$$u_z(r, \theta, 0) = -u_z\left(r, \theta, \frac{L}{N_a}\right), \quad (2)$$

where  $u_\theta$  is the displacement in  $\theta$ ,  $u_z$  is the displacement in  $z$  and  $N_a$  is the number of cells in the axial direction

$$u_r\left(\frac{D_i}{2}, \theta, z\right) = \begin{cases} \frac{(D_f - D_i)\pi}{N_c} \\ 'free' \\ -\frac{1}{4} \frac{(D_f - D_i)\pi}{N_c} \end{cases} \quad (3)$$

where  $u_r$  is the displacement in  $r$ , and  $D_f, D_i, N_c$  are listed in Table 2.  $N_c$  is the number of cells in the circumferential direction. The first stage consists of a load corresponding to a stent expansion from  $D_i$  to  $D_f$ . In the second stage, the load is removed to allow for elastic recoil, hence the 'free' boundary condition. Finally, the third stage consists of decreasing the diameter to 25% of the initial diameter change. The finite element solutions obtained from the first, second and third stages, are used to determine respectively foreshortening, recoil and radial stiffness.

#### 3.2.1 Structural performance metrics

The structural metrics considered in this work are foreshortening, elastic recoil and radial stiffness. Small foreshortening improves the placement accuracy of the stent. A low elastic recoil helps to achieve a more accurate final stent diameter. Finally, a high radial stiffness prevents the blood vessel to close under load.

The foreshortening is defined as the ratio of the change in the length of the stent during the first stage to the initial length before balloon expansion.

$$\partial l = \frac{L_{load} - L_{unload}}{L_{load}}. \quad (4)$$

Elastic recoil is defined as the ratio of the change in radius of the stent during the second stage to the radius before the load is removed.

$$R_e = \frac{R_{load} - R_{unload}}{R_{load}}. \quad (5)$$



The radial stiffness is defined as the ratio of the change in pressure on the outside of the stent to the change in radial strain during the third stage.

$$D_R = \frac{\Delta P}{\Delta \epsilon_R}. \quad (6)$$

### 3.3 Computational fluid dynamics model for blood flow analysis through stented vessel

Previous studies have modelled blood as either a Newtonian or non-Newtonian fluid in an attempt to balance accuracy with computational cost. In this study, blood is assumed to be Newtonian with constant viscosity. The assumption of blood as Newtonian underestimates the WSS and can thus overestimate the risk of restenosis [40]. Therefore the hemodynamic performance of a stent, and any newly design stents, will perform better than the modelling results here presented suggest. In addition, our motivation is that this analysis model will be used in a future optimization study, for which it is imperative to keep computational cost low. The strategy here is to model the flow over one RVE and compare the results to those obtained from analysing the flow over an entire stent.

A geometry, created from the deformed mesh, is used to perform an extruded cut in the fluid domain followed by a tessellation. An extrusion of 5 mm was added at the inlet to prevent a discontinuity from the applied inlet condition at the wall. ANSYS software package (ANSYS, USA) was used to create the finite element model. The fluid domain was meshed in ICFM CFD. A typical velocity profile in the near-wall region undergoes large variations in the direction normal to the wall. Fluid velocity near the wall needs to be computed accurately to determine the wall shear stress. Therefore, the mesh at the wall must be finer than in the rest of the computational domain. Placing a finer-resolution mesh grid near the wall without subjecting the whole mesh to the chosen resolution is known as inflation. In this CFD model, an inflation mesh of 10 layers was imposed on the wall. The resulting mesh was then used in FLUENT (ANSYS, USA) to model blood flow over the stent. The blood fluid properties used were: a density of 1080 kg/m<sup>3</sup> and a viscosity of 0.0035 Pa.s [41]. An inlet velocity profile corresponding to a Poiseuille flow of Re=500 was applied. This corresponds to the average Reynold's number of an 18mm diameter artery [24]. A no-slip boundary condition was applied at the wall, and a pressure boundary condition was applied at the outlet. Symmetric boundary conditions were also applied at the remaining sides.

#### 3.3.1 Mathematical formulation of the wall shear stress index

Mejia et al. [24] used the first, second and fourth statistical spatial moments of the WSS distribution between struts to assess the hemodynamic performance of stents with varying strut profiles. In order to assess the hemodynamic compatibility of alternative stent geometries, the distribution of WSS inside the stent cell must be evaluated instead. The three main moments relevant to our investigations are the second, third and fourth spatial moment, known as variance ( $\Sigma$ ), skewness ( $sk$ ) and kurtosis ( $K$ ). They describe respectively the spread, skewness and “peakedness” of a probability distribution. The mean is ignored since it describes a location in the WSS distribution.

To characterise the distribution of the wall shear stress with a single value and include the effects of all three statistical moments, we define here a wall shear stress index by taking their normalized average:

$$WSS_I = \frac{1}{3} \left( \overline{\|\Sigma\|} + \frac{1}{sk} + \frac{1}{K} \right), \quad (7)$$

where  $\overline{\|\Sigma\|} = \frac{\|\Sigma\|}{\|\Sigma_{ideal}\|}$ ,  $\overline{sk} = \frac{sk}{sk_{ideal}}$  and  $\overline{K} = \frac{K}{K_{ideal}}$  with  $\Sigma_{ideal}$ ,  $sk_{ideal}$  and  $K_{ideal}$  being the statistical moments of the ideal distribution with the same geometry. A weighted arithmetic mean is chosen so that not all moments contribute equally to the  $WSS_I$  [42].

The value  $WSS_I$  can assume varies between 0 and 1. A stent with a better hemodynamic performance will have a higher value of  $WSS_I$ , 1 being the ideal case. This definition allows for the characterization of the hemodynamic compatibility with a single value, a factor that can be advantageous during iterative computational processes, such as those often required in optimization. However, a factor not taking into account here is that  $WSS_I$  is an average measure. It cannot capture if one of the statistical moments might show more variation with hemodynamic compatibility than the rest.

## 4 Results and discussion

This section presents the results obtained from the structural and hemodynamic models described in Section 3. We use the stent metrics to assess stent performance of the cell topologies illustrated in Table 1. The results obtained from the RVE scheme are compared with those obtained by detailed computations of the entire stent. The advantage of using the RVE method will be demonstrated, together with a discussion of the accuracy and limitations of the method.

### 4.1 Structural metrics

Figures 2, 3 and 4 present the results obtained from the analysis of the stents described in Section 3. A detailed 3D finite element model of the entire stents was also developed to compare the results with those obtained with the RVE approach. The same elastoplastic material property specified in Section 3 is used. The three-stage load described in Section 3.2 and used in Eq. (3) is applied.

The results show that the absolute foreshortening of the “Auxetic” stent is the highest, followed by the “Diamond” stent. The “Auxetic” unit cell exhibits a negative Poisson’s ratio. Thus when expanded, the “Auxetic” stent lengthens, resulting in a negative foreshortening. The hybrid stents have close to zero absolute foreshortening. This is expected as the hybrid stents both consist of regular hexagonal units and re-entrant hexagonal units. The regular hexagon exhibits a positive Poisson’s ratio, whereas the other, a negative Poisson’s ratio. Moreover, the “Hybrid C” has a foreshortening closest to zero due to the struts that run longitudinally down the stent, as shown in Fig. 5. The “Chevron B” stent has 2 pairs of bending struts in its unit cell that deform similarly during stent expansion. This geometry results in the horizontal struts in the middle to displace by an equal amount during stent expansion. Since the left and right boundary of the RVE move accordingly, there is no resultant change in the length of the stent. This mechanism is highlighted in Fig. 6.



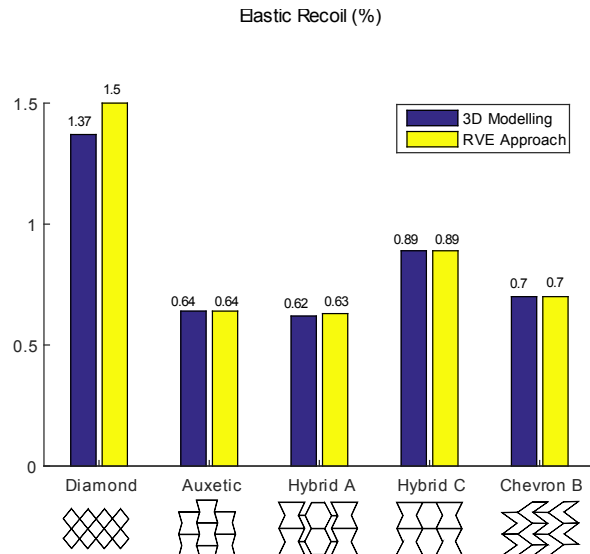


Figure 2: Elastic Recoil - 3D Modelling vs. RVE Approach

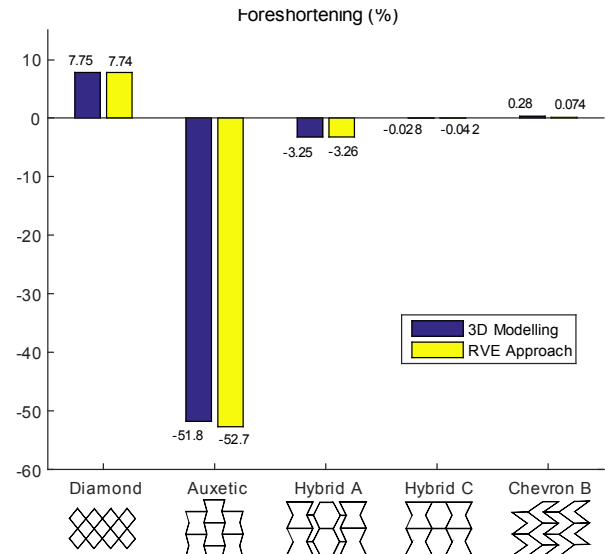


Figure 3: Foreshortening - 3D Modelling vs. RVE Approach

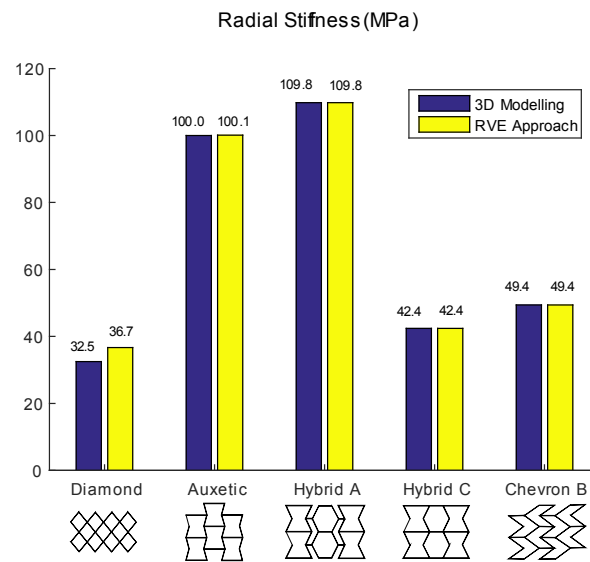


Figure 4: Radial Stiffness - 3D Modelling vs. RVE Approach

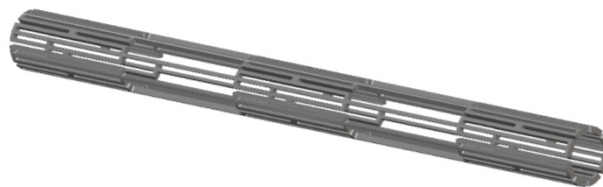


Figure 5: "Hybrid C" Stent

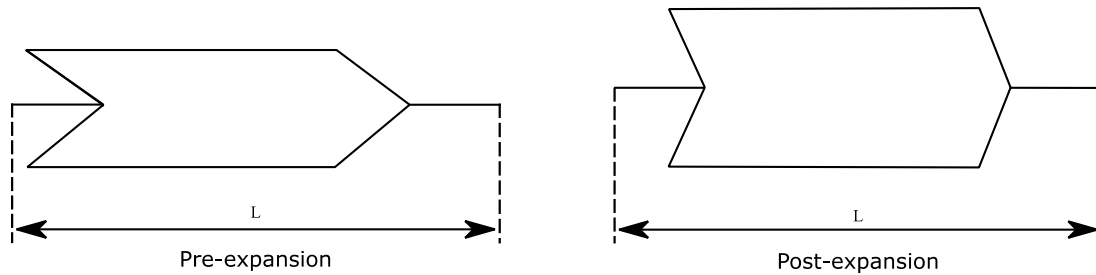


Figure 6: "Chevron B" Expansion Mechanism

The amount of elastic recoil experienced by each stent is relatively invariant, with the exception of that of the "Diamond" stent. The "Hybrid A" stent has the lowest recoil, and the "Diamond" stent has the highest. This implies that during expansion the "Hybrid A" stent will require less balloon over-inflation in order to achieve the target diameter.

Figures 2, 3 and 4 show a good agreement between the results obtained from the entire stent model and the RVE approach. The non-zero stents metrics exhibit errors of less than 15%. The higher difference is observed for the evaluation of the elastic recoil and the radial stiffness of the "Diamond" stent. This disparity stems from the application of periodic boundary conditions to the RVE. This implies that the periodicity assumption holds only for lattices of relatively large size, which is not the case here. Thus, if the stent experiences significant deformation at each end, the results may be influenced, as for the case of the "Diamond" stent, which contains the hinge of a bending strut on the RVE boundary.

A large variation is also noted in the evaluation of the foreshortening of the "Hybrid C" and "Chevron B" stents. These results suggest that the RVE method is not appropriate to assess a property when its value approaches zero. However, since foreshortening and recoil will be constrained to be non-zero in design optimization formulations, the RVE approach will be sufficient to evaluate these stent metrics.

Figure 4 also shows that the "Hybrid A" stent has a higher radial stiffness, as opposed to the "Diamond" one, which has the lowest. In general, the radial stiffness of a stent depends mainly on the number of bending dominated struts after stent expansion. This number is the highest for the "Diamond" and "Auxetic" stents, namely 20 along one row of cells. In contrast, this number decreases to 16 for the "Hybrid A" stent and finally to 12 for the "Hybrid C" and "Chevron B" stents. Hence with except to the "Diamond" stent, the number of bending dominated struts along one row can be correlated with the radial stiffness of each stent. Based on this correlation, the "Diamond" stent should exhibit a radial stiffness of the order of 100 MPa. As seen in Fig. 4, this is not the case. The reason is that the radial stiffness is also heavily affected by the stent strut angle, the angle between bending-dominated struts and the axial direction. The stent strut angle is lower for the "Diamond" stent, for which a lower bending moment would be required to bend the struts, resulting in a lower radial stiffness. This implies that the number of unit cells along the circumferential direction has a large impact on the radial stiffness. For a given change in diameter of the expanded stent, a lower number of cells along the circumferential direction results in a larger rotation of stents with bending-dominated cells. After expansion, the stent strut angles becomes closer to  $90^\circ$ , thereby stiffening radially the stent. As a result, a decrease in the number of cells along the circumferential direction can be used as a strategy to stiffen the stent. Also, for the "Diamond" stent, the strut angle can be increased by expanding the stent further. However, this will come at a cost of increasing the foreshortening of the "Diamond" stent.

The number of bending dominated struts has also a significant impact on the elastic recoil. The presence of bending dominated struts with a lower strut angle results in a higher elastic recoil, as seen for the "Diamond" stent. When the radial load is removed during the recoil step, the bending-dominated struts

will experience a decrease in the stent strut angle. A large cell strut angle after stent expansion therefore results in a low elastic recoil and vice versa.

The results of this section on the stent expansion mechanisms and relative structural metrics show that the stent properties are strongly influenced by the topology of the unit cell and the stent size. In addition, we can infer that an RVE method is effective in evaluating the structural stent metrics as long as the stent geometry respects certain assumptions.

#### **4.2 Hemodynamic performance**

The ideal WSS distribution is one that is achieved without the presence of the stent, which corresponds to the constant wall shear stress of the physiological value. Here, the hemodynamic performance of a stent is assessed by calculating the percentage area of the arterial wall exposed to a wall shear lower than 5% of the physiological value. Figure 7 depicts the results obtained for all the stents with respect to the percentage area of the arterial wall exposed to critical WSS. The  $WSS_l$  for the stents with more than one unit cells was calculated by taking the average of the  $WSS_l$  of each unit cell.

The results confirm that the “Chevron B” unit cell performs better than the other stents with only 8.9% of the arterial wall exposed to WSS, lower than 10% the physiological value. This is mainly determined by the relatively large size of the unit cell of the “Chevron B” stent. A large unit cell results in the presence of fewer struts in the direction of the flow, thereby allowing the velocity profile to redevelop for a longer distance. Since regions of low wall shear stresses occur around the struts, this results in a better hemodynamic performance.

Figure 7 also shows a clear correlation between the normalised variance and the hemodynamic performance of the stents. The normalised skewness and kurtosis however do not. The values for the “Diamond” and “Hybrid C” unit cells do not follow the expected pattern. Nevertheless, the  $WSS_l$  assesses the stents hemodynamic performance correctly.

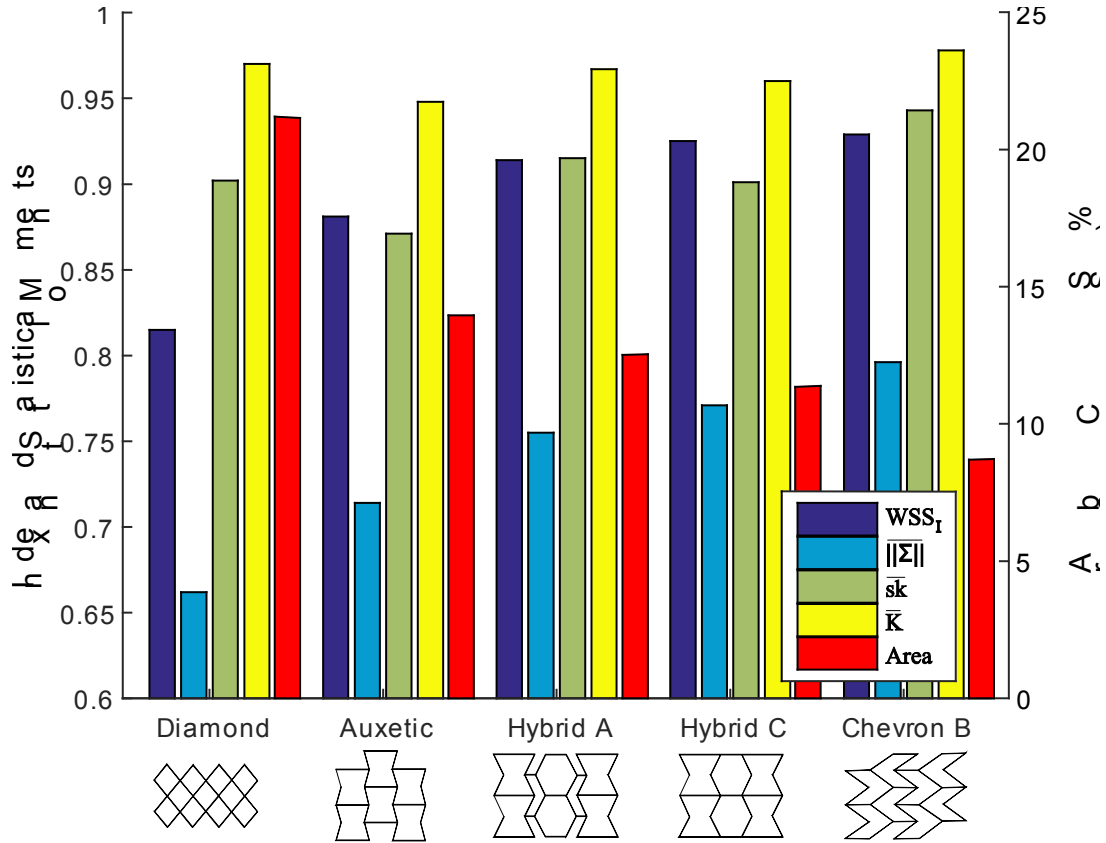


Figure 7: Overall performance of each stent based on the wall shear stress index ( $WSS_I$ ), normalized variance ( $||\Sigma||$ ), skewness ( $s_k$ ) and kurtosis ( $K$ )

The results of this section show that the metric defined here,  $WSS_I$  given by equation (7), can be used by a clinician to assess the hemodynamic performance of a particular stent design with geometry that can be reduced to that of a periodic lattice. A clear correlation with the  $WSS_I$  and the area exposed to critical WSS can be observed. As the area exposed to critical WSS decreases,  $WSS_I$  increases. In this case, the “Chevron B” stent is less likely to result in restenosis after the stenting procedure. In addition, this work sets the foundation for a design optimization study to obtain stent designs with improved radial stiffness and hemodynamic performance. The goal would be to design stents that can support greater loads while simultaneously lower the risk of restenosis.

Figure 8 summarises the results of the structural and hemodynamic metrics obtained for all considered stents. It can be observed that the hemodynamic performance and the radial stiffness do not follow a similar trend. Except for the properties of the “Diamond” stent, the two metrics are generally conflicting, i.e., as  $WSS_I$  increases, radial stiffness decreases. This shows that there is a possibility to obtain optimised stent designs with improved radial stiffness and hemodynamic performance through multi-objective optimization. Overall, the “Hybrid A,” “Hybrid C” and “Chevron B” stents are the best-performing stents; they have high hemodynamic performance and low foreshortening. Therefore, the use of these stent designs will lower the risk of restenosis and increase placement accuracy. The “Auxetic” stent may damage the blood vessel during insertion due to its high foreshortening. It is important to note that the RVE approach here presented is helpful to develop structural and hemodynamic metrics for comparing alternative stent designs with initial geometry that can be reduced

to that of periodic lattices as further explained below. The methodology here proposed is not intended to model or predict long-term performance of deployed stents.

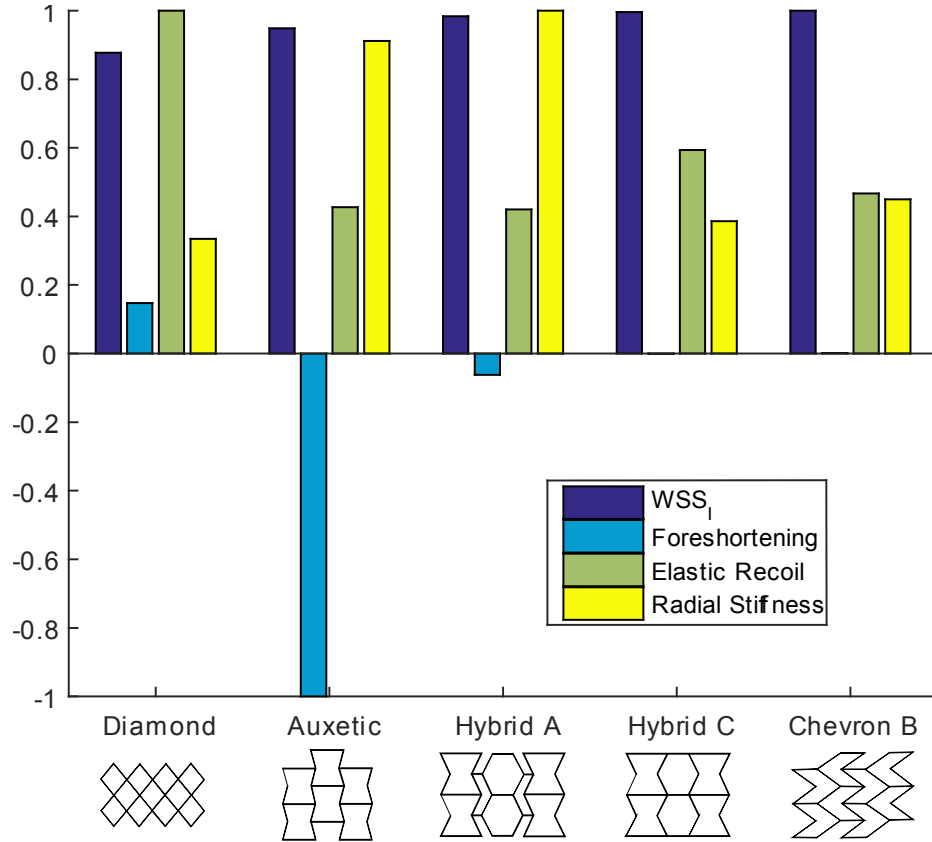


Figure 8: Normalised Hemodynamic Performance and Stent Metrics

The purpose of this work is to evaluate the performance of a stent by evaluating the structural properties and hemodynamic compatibility using an RVE approach. Several clinical reports have highlighted the challenge foreshortening poses to accurate stent placement [43-46]. Stents that shorten can result in the clinician missing the target zone resulting in the deployment of a secondary stent. Stents with low elongation on expansion have had a lower reported incidence and rate of restenosis compared to other bare-metal stents [47-50]. Restenosis has also been linked to the change in blood flow around the stent [23]. Our results show that using an RVE method, such as that presented in this work, is effective in evaluating clinically relevant properties of stents. Furthermore, this approach helps in providing clinically relevant metrics to compare alternative stent designs that are available in the cardiovascular market. On the other hand, this method can be used only for periodic geometries that can be reduced to a repeated unit where the following kinematic assumptions hold

- the periodic directions of the stent change according to the macroscopic displacement gradient
- the stent remains periodic during deformation

For patient-specific designs that involve alteration of the periodicity or for stents that are no longer periodic after deformation, this approach has limitations and require extensions that are beyond the scope of this paper.

## 5 Conclusion

This work has quantified structural metrics and hemodynamic performance of stents modelled as periodic lattices. We have shown that the former, i.e. foreshortening, elastic recoil, and radial stiffness, can be calculated via an RVE approach, whereas the latter can be defined by a wall shear stress index assessed with a statistical approach. The results have shown that each cell topology has its own structural and hemodynamic performance, which can be used to compare and select the stent geometry that best trades off the clinical requirements.

## 6 References

1. Mozaffarian, D., et al., *Heart disease and stroke statistics--2015 update: a report from the American Heart Association*. Circulation, 2015. **131**(4): p. 29-322.
2. Kraitzer, A., Y. Kloog, and M. Zilberman, *Approaches for prevention of restenosis*. J Biomed Mater Res B Appl Biomater, 2008. **85**(2): p. 583-603.
3. LaDisa, J.F., Jr., et al., *Alterations in wall shear stress predict sites of neointimal hyperplasia after stent implantation in rabbit iliac arteries*. Am J Physiol Heart Circ Physiol, 2005. **288**(5): p. H2465-75.
4. Papafaklis, M.I., et al., *Relationship of shear stress with in-stent restenosis: bare metal stenting and the effect of brachytherapy*. Int J Cardiol, 2009. **134**(1): p. 25-32.
5. Sanmartin, M., et al., *Influence of shear stress on in-stent restenosis: In vivo study using 3D reconstruction and computational fluid dynamics*. Revista Espanola De Cardiologia, 2006. **59**(1): p. 20-27.
6. Wentzel, J.J., et al., *Relationship between neointimal thickness and shear stress after wallstent implantation in human coronary arteries*. Circulation, 2001. **103**(13): p. 1740-1745.
7. Serruys, P.W. and R. Benno, *Handbook of coronary stents*. 2002, London; Florence, KY, USA: Martin Dunitz ; Taylor & Francis.
8. Duerig, T.W. and M. Wholey, *A comparison of balloon- and self-expanding stents*. Minim Invasive Ther Allied Technol, 2002. **11**(4): p. 173-8.
9. De Beule, M., et al., *Realistic finite element-based stent design: the impact of balloon folding*. J Biomech, 2008. **41**(2): p. 383-9.
10. Wang, W.Q., et al., *Analysis of the transient expansion behavior and design optimization of coronary stents by finite element method*. J Biomech, 2006. **39**(1): p. 21-32.
11. Zahora, J., A. Bezrouk, and J. Hanus, *Models of stents - comparison and applications*. Physiol Res, 2007. **56 Suppl 1**: p. S115-21.
12. Tan, L.B., et al., *A method for investigating the mechanical properties of intracoronary stents using finite element numerical simulation*. Int J Cardiol, 2001. **78**(1): p. 51-67.
13. Holzapfel, G.A., M. Stadler, and T.C. Gasser, *Changes in the mechanical environment of stenotic arteries during interaction with stents: computational assessment of parametric stent designs*. J Biomech Eng, 2005. **127**(1): p. 166-80.
14. Tan, T.W., et al., *Compliance and Longitudinal Strain of Cardiovascular Stents: Influence of Cell Geometry*. Journal of Medical Devices-Transactions of the Asme, 2011. **5**(4): p. 041002.

15. Pant, S., N.W. Bressloff, and G. Limbert, *Geometry parameterization and multidisciplinary constrained optimization of coronary stents*. Biomechanics and modeling in mechanobiology, 2012. **11**(1-2): p. 61-82.
16. Martin, D. and F. Boyle, *Computational structural modelling of coronary stent deployment: a review*. comput methods biomech biomed engin Computer Methods in Biomechanics and Biomedical Engineering, 2011. **14**(4): p. 331-348.
17. Grogan, J.A., S.B. Leen, and P.E. McHugh, *Comparing coronary stent material performance on a common geometric platform through simulated bench testing*. Journal of the Mechanical Behavior of Biomedical Materials Journal of the Mechanical Behavior of Biomedical Materials, 2012. **12**(5): p. 129-138.
18. Hongxia, L., et al., *Design optimization of stent and its dilatation balloon using kriging surrogate model*. BioMedical Engineering OnLine, 2017. **16**: p. 13.
19. Douglas, G.R., A.S. Phani, and J. Gagnon, *Analyses and design of expansion mechanisms of balloon expandable vascular stents*. J Biomech, 2014. **47**(6): p. 1438-46.
20. Masoumi Khalil Abad, E., D. Pasini, and R. Cecere, *Shape optimization of stress concentration-free lattice for self-expandable Nitinol stent-grafts*. J Biomech, 2012. **45**(6): p. 1028-35.
21. Thury, A., et al., *Images in cardiovascular medicine. Focal in-stent restenosis near step-up: roles of low and oscillating shear stress?* Circulation, 2002. **105**(23): p. e185-7.
22. Malek, A.M., S.L. Alper, and S. Izumo, *Hemodynamic shear stress and its role in atherosclerosis*. Journal of American Medical Association, 1999. **282**(21): p. 2035-42.
23. LaDisa, J.F., Jr., et al., *Three-dimensional computational fluid dynamics modeling of alterations in coronary wall shear stress produced by stent implantation*. Ann Biomed Eng, 2003. **31**(8): p. 972-80.
24. Mejia, J., et al., *Evaluation of the effect of stent strut profile on shear stress distribution using statistical moments*. BioMedical Engineering OnLine, 2009. **8**: p. 8.
25. Balossino, R., et al., *Effects of different stent designs on local hemodynamics in stented arteries*. J Biomech, 2008. **41**(5): p. 1053-61.
26. Frank, A.O., P.W. Walsh, and J.E. Moore, Jr., *Computational fluid dynamics and stent design*. Artif Organs, 2002. **26**(7): p. 614-21.
27. Johnston, B.M., et al., *Non-Newtonian blood flow in human right coronary arteries: transient simulations*. J Biomech, 2006. **39**(6): p. 1116-28.
28. Hao-Ming, H., et al., *Cardiovascular stent design and wall shear stress distribution in coronary stented arteries*. Micro and Nano Letters, 2012. **7**(5): p. 430-433.
29. LaDisa, J.F., Jr., et al., *Circumferential vascular deformation after stent implantation alters wall shear stress evaluated with time-dependent 3D computational fluid dynamics models*. Journal of Applied Physiology, 2005. **98**(3): p. 947-57.
30. Khanoki, S.A., and Pasini, D., *Mechanical properties of lattice materials via asymptotic homogenization and comparison with alternative homogenization methods*. International Journal of Mechanical Science, 2013.
31. Khanoki, S.A. and D. Pasini, *The Fatigue Design of a Bone Preserving Hip Implant With Functionally Graded Cellular Material*. Journal of Medical Devices-Transactions of the Asme, 2013. **7**(2).
32. Masoumi Khalil Abad, E., S. Arabnejad Khanoki, and D. Pasini, *Fatigue design of lattice materials via computational mechanics: Application to lattices with smooth transitions in cell geometry*. International Journal of Fatigue, 2013. **47**: p. 126-136.

33. Vigliotti, A., V.S. Deshpande, and D. Pasini, *Non linear constitutive models for lattice materials*. Journal of the Mechanics and Physics of Solids, 2014. **64**(0): p. 44-60.
34. Vigliotti, A. and D. Pasini, *Linear multiscale analysis and finite element validation of stretching and bending dominated lattice materials*. Mechanics of Materials, 2012. **46**(0): p. 57-68.
35. Vigliotti, A. and D. Pasini, *Stiffness and strength of tridimensional periodic lattices*. CMA Computer Methods in Applied Mechanics and Engineering, 2012. **229-232**: p. 27-43.
36. Vigliotti, A. and D. Pasini, *Mechanical properties of hierarchical lattices*. Mechanics of Materials, 2013. **62**(0): p. 32-43.
37. Elsayed, M.S.A. and D. Pasini, *Multiscale structural design of columns made of regular octet-truss lattice material*. International Journal of Solids and Structures International Journal of Solids and Structures, 2010. **47**(14-15): p. 1764-1774.
38. Elsayed, M.S.A. and D. Pasini, *Analysis of the elastostatic specific stiffness of 2D stretching-dominated lattice materials*. Mechanics of Materials Mechanics of Materials, 2010. **42**(7): p. 709-725.
39. Levesque, J., et al., *Materials and properties for coronary stents*. Advanced Materials and Processes, 2004. **162**(9): p. 45-48.
40. Mejia, J., R. Mongrain, and O.F. Bertrand, *Accurate prediction of wall shear stress in a stented artery: Newtonian versus non-newtonian models*. Journal of Biomechanical Engineering, 2011. **133**(7).
41. Smadi, O., et al., *Numerical and experimental investigations of pulsatile blood flow pattern through a dysfunctional mechanical heart valve*. Journal of Biomechanics, 2010. **43**(8): p. 1565-1572.
42. Beliakov, G., H. Bustince Sola, and T. Calvo Sánchez, *A practical guide to averaging functions*. 2016.
43. Beek, F.J.A., et al., *Complications during renal artery stent placement for atherosclerotic ostial stenosis*. CardioVascular and Interventional Radiology, 1997. **20**(3): p. 184-190.
44. Aytekin, C., et al., *Endovascular stent placement in the treatment of upper extremity central venous obstruction in hemodialysis patients*. European Journal of Radiology. **49**(1): p. 81-85.
45. Forbes, T.J., et al., *The Genesis stent: A new low-profile stent for use in infants, children, and adults with congenital heart disease*. Catheterization and Cardiovascular Interventions, 2003. **59**(3): p. 406-414.
46. Cheatham, J.P., *Stenting of coarctation of the aorta*. Catheterization and Cardiovascular Interventions, 2001. **54**(1): p. 112-125.
47. Hoffmann, R., et al., *Relation of stent design and stent surface material to subsequent in-stent intimal hyperplasia in coronary arteries determined by intravascular ultrasound*. American Journal of Cardiology. **89**(12): p. 1360-1364.
48. Hara, H., et al., *Role of stent design and coatings on restenosis and thrombosis*. Advanced Drug Delivery Reviews, 2006. **58**(3): p. 377-386.
49. Yoshitomi, Y., et al., *Does stent design affect probability of restenosis? A randomized trial comparing Multilink stents with GFX stents*. American Heart Journal. **142**(3): p. 445-451.
50. Kastrati, A., et al., *Restenosis after coronary placement of various stent types*. American Journal of Cardiology. **87**(1): p. 34-39.